IEEE Open Journal of
Circuits and Systems

Received 25 August 2022; revised 21 October 2022; accepted 24 October 2022. Date of current version 23 November 2022.
This article was recommended by Associate Editor M. Wang.

Digital Object Identifier 10.1109/OJCAS.2022.3218823

Control Strategy of Three-Level NPC Inverter Based on Variable Coefficient Virtual Vector Model Predictive Control

WEIQUAN GU[1], HUANGZHENG LIAO[2], JIAQI LIN[2], ZEWEN LI[3], AND TAO JIN[2] (Senior Member, IEEE)

[1]Deptartment of Science and Technology, Fujian Fuqing Nuclear Power Company Ltd., Fuqing 350318, China

[2]College of Electrical Engineering and Automation, Fuzhou University, Fuzhou 350116, China

[3]Department of Equipment Center, State Grid Fujian Electric Power Research Institute, Fuzhou 350116, China

CORRESPONDING AUTHORS: Z. LI and T. JIN (e-mail: 453583542@qq.com; jintly@fzu.edu.cn)

This work was supported in part by the Chinese National Natural Science Foundation under Grant 51977039, and in part by The Central Government Guiding Local Science and Technology Development Project under Grant 2021L3005.

ABSTRACT The Conventional model predictive control (C-MPC) uses only a single voltage vector in each control period, resulting in poor control performance. In addition, the computational burden in discrete space state generated by three-level inverter cannot be ignored. To improve the control performance, this paper proposes a variable coefficient virtual vector MPC (VC-VV-MPC) method, a five-level virtual space voltage vector is constructed to improve the control performance, and a scaling coefficient is used to further improve the control performance. In addition, a voltage vector pre-selection method is used to reduce the computational burden. The simulation and experiment results shown that, compare with C-MPC and adjacent vector MPC (AV-MPC), the proposed VC-VV-MPC can achieve the improvement of control performance under lower computational burden.

INDEX TERMS Model predictive control (MPC), variable coefficient, virtual vector, computational burden, three-level NPC inverter.

I. INTRODUCTION

IN RECENT years, with the development of renewable energy, the capacity and voltage level of renewable energy equipment are gradually increased, related inverters with capacity reaching several MW have been developed rapidly. Among these multi-megawatt converters, the three-level neutral point clamped topology is a promising solution which has been widely adopted in many product lines [1] in renewable energy due to its ability to operate at medium voltage and with multi-level voltage characteristics leading to high power quality compare to two-level converters [2].

Most power converters in renewable energy require a control unit which is traditionally implemented using proportional integral regulator both inner and outer loops. However, such approach requires a proper method for tuning control parameters and difficulties to include non-linearity of the plant in the control design. Therefore, it is challenging is to control converter applied in renewable energy guaranty stability in wide operating points [3]. To solve these problems, advanced control algorithms have been proposed in the literature [4], [5]. Among them, finite-set model predictive control (MPC) has gained many attentions because of simplicity and possibility to include non-linear and multiple control objectives [6]. In the conventional MPC (C-MPC), the core idea is to use the discrete current prediction mathematical model and voltage vector (VV) to predict the output current of the next sample, then choose the optimal VV [7], [8], [9], [10]. C-MPC has been found suitable for two-level converter where the number of vectors is limited to 7. But its main drawbacks related with the short sampling time requirements as well as variable switching frequency and computation time has limited its wide acceptance for multilevel converters [19], [20], [21]. For the three-level inverter, it was found that, C-MPC needs

to evaluate 27 VVs per control period, result to poor output THD performance and large current ripple [11], [12], [13]. Moreover, its large amount of computation, makes it difficult to implement in a DSP/FPGA control hardware. Recently, improved C-MPC methods suitable for three-level converters have been proposed in [14], [15], [16].

To solve the computation problem of C-MPC, the research work in [14] has proposed a computationally efficient direct MPC with hexagon control region and triangle control region method (CE-MPC with HCR and CE-MPC with TCR). In this approach, the computation is optimized by using the method of reference control VV and the optimization algorithm of different sub-regions. This work was evaluated through experiments which show that CE-MPC with TCR has the best performance in terms of computation optimization and THD performance [14]. The literature [15] has proposed an improved method based on look up table to reduce the calculation time for the matrix converter. For the purpose of reducing the amount of computation brought by C-MPC method, this paper divides the whole space vector graph into six sectors, and selects 10 candidate vectors based on look up table to calculate the cost function. The experimental results show that the computational complexity of the proposed method is much lower than that of the C-MPC method [15]. Research work in [16] proposed a Generalized Adjacent Vectors (AV-MPC) method to reduce the computation, it provides three subsets for a given number of converter level, then choose the adjacent vector of best vector at last moment, to participate in calculation [16]. Experiment have proved the feasibility of this proposed method.

For the purpose of improving the steady-state and THD performances of the C-MPC method, the usual method is increasing the control frequency or filter size. However, due to the large computation of C-MPC, it is not easy to increase the control frequency, and if the filter is increased, the volume of the whole system will increase. Therefore, the modulated MPC (M-MPC) to improve the steady-state output performances was proposed in [17]. In this method the reference control VV is calculated, then find the best of three adjacent vectors [17]. According to the vector composition principle, the time of each vector, t_1, t_2 and t_3, is calculated then transformed to gate signals and output voltage of converter. This method can effectively improve the output THD performance, but its online calculation of the switching duration increases the complexity of the control algorithm. MPC based on a double vector method is proposed in [18] to improve the comprehensive performance of the C-MPC. The method in [18] of double vector synthesis is used to determine the size sector of the optimal voltage switching vector. After the small triangle region of the optimal vector is determined, two adjacent vectors are used to synthesize the control. In order to reduce the computational burden of dual vector synthesis, this method make the two vectors work for half of each period but this also limit the improvement of the output performance. Experimental results and comparisons analysis with discussion in [18] show that the double vector method can improve the output THD performance greatly and reduce the common-mode voltage effectively.

Aiming to select the best control algorithm among various approach existed in the literature, this paper evaluates three strategies including the newly proposed algorithm named variable coefficient virtual vector model predictive control (VC-VV-MPC). This method combines the concept of equivalent action time of the PWM modulation strategy, making the output voltage level of the MPC non-integer. In this way, the output current ripple of the MPC can be effectively reduced, and the THD performance can also be improved after the introduction of the virtual vector. The other methods selected for comparison are C-MPC and AV-MPC method. Comparative analysis is mainly aimed at THD performance, capacitance balance and calculation time.

The contributions made by this article mainly include the following three aspects:

(1) This paper introduces the concept of equivalent action time, then introduce five-level space vector into three-level inverter control. Through the coefficient, three level space vector can be transformed to five level space vector. It also can extend to higher level in reverse. However, increased virtual voltage state vector will increase calculation time of per control period. This paper adopts the ideal voltage vector calculation and sub-sector method to reduce the calculation of conventional model predictive control method.

(2) This paper introduces a variable coefficient to the VV to be selected, it aims to solve the difference between high and low reference current.

(3) Verification of three control algorithms through simulation and experimental platform consisting of a 1 kW three-level NPC inverter driven by a TMS320F28379D control unit. The results have shown that, the proposed method provide superior performances in terms of reduced THD and computation.

The rest of this paper is organized as follows: C-MPC is present in Section II. Section III discusses on the proposed virtual vector algorithm based on variable coefficient. Simulation and experimental results are discussed in Section IV. After that, finally conclusion is given in Section V.

II. C-MPC METHOD OF THREE-LEVEL NPC INVERTER

Fig. 1 shows the structure of neutral point clamped (NPC) three-level three-phase off-grid inverter

The three-level NPC off-grid inverter is composed of a DC voltage source V_{dc} on the DC side, two DC capacitor C_{dc}, three-level NPC converter, L-type filters L, line resistance R_{L} and load resistance R_{o}. For a three-level NPC inverter, each phase has three switching states. For example, when S_{a1} and S_{a2} are turned on, the output voltage is $V_{\mathrm{dc}}/2$, the switching state is 1. When S_{a1} is turned off and S_{a2} is turned on, the output voltage is 0, the switching state is 0. When S_{a1} and S_{a2} are both in the off state, the output voltage is

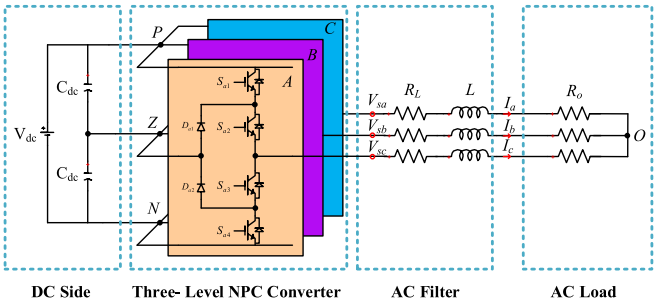

FIGURE 1. The structure of NPC off-grid inverter.

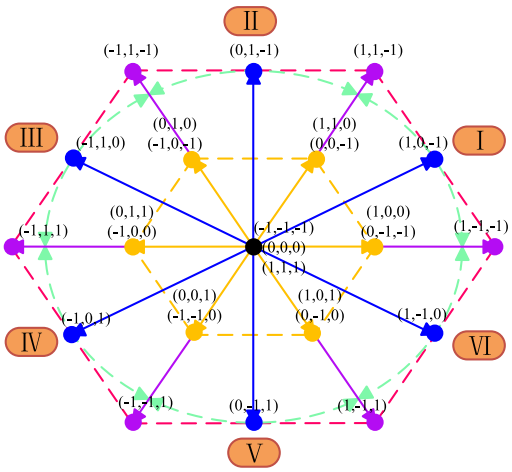

FIGURE 2. Three-level space vector diagram.

$-V_{\rm dc}/2$, the switching state is -1. Therefore, the three-level space vector of NPC inverter is shown in Fig. 2.

According to KVL, the mathematical model of three-level NPC inverter output side is as follows

$$\begin{cases} Vs_a = L\frac{dI_a}{dt} + R_L I_a + R_o I_a \\ Vs_b = L\frac{dI_b}{dt} + R_L I_b + R_o I_b \\ Vs_c = L\frac{dI_c}{dt} + R_L I_c + R_o I_c \end{cases} \tag{1}$$

where

Vs_a, Vs_b, Vs_c	The output voltages of three phase NPC converter
I_a, I_b, I_c	The output currents of three phase NPC converter
L	Line inductance
R_L	Line resistance
R_o	Load resistance

First, list the KVL equation of the three-phase NPC inverter, as shown in equation (1). Then discrete the KVL equation of three-level inverter, and then use 3-2 transformation to get the following current prediction equation.

$$\begin{cases} I_\alpha^{k+1} = (1-(R_O+R_L)T_s/L)I_\alpha^k \\ \quad +T_s\left(V_\alpha - I_\alpha^k(R_O+R_L)\right)/L \\ I_\beta^{k+1} = (1-(R_O+R_L)T_s/L)I_\beta^k \\ \quad +T_s\left(V_\beta - I_\beta^k(R_O+R_L)\right)/L \end{cases} \tag{2}$$

where

I_α^k, I_β^k	α-β axis converter current at k moment;
$I_\alpha^{k+1}, I_\beta^{k+1}$	α-β axis converter current at k + 1 moment;
V_α^k, V_β^k	α-β axis converter voltage at k moment;
T_s	Control period;

In order to obtain the predicted current I_α^{k+1} and I_β^{k+1}, it is necessary to sample current value I_α^k and I_β^k, then use the switch state vector V_α^k and V_β^k to calculate predicted current. Apart from the current tracking control, the three-level NPC inverter also needs to solve capacitor voltage unbalanced problem between upper and lower capacitor of DC side. The voltage fluctuation is determined by the current I_O flowing through the neutral point. Among the three-level space vectors in Fig. 2, only small vectors will affect the neutral point voltage balance. The specific calculation equation is as follow.

$$\Delta\, V_{dc}{=}V_{dc-upper} - V_{dc-lower} = \frac{1}{2C_{\rm dc}}\int (S_a I_a + S_b I_b + S_c I_c)dt \tag{3}$$

where

$V_{dc-upper}$, $V_{dc-lower}$	Voltage of upper and lower capacitors.
S_a, S_b, S_c	Converter output level.
C_{dc}	DC bus capacitance.
ΔV_{dc}	Capacitance voltage difference between upper and lower capacitance.

To get the optimal VV, it is need to calculate the cost function of each voltage vector to find the optimal switching vector. It is not only calculated the current tracking error, but also need consider the voltage balanced. So, the cost function normally is like equation (4).

$$G = |I_{\alpha-ref}^{k+1} - I_\alpha^{k+1}| + |I_{\beta-ref}^{k+1} - I_\beta^{k+1}| + \lambda|\Delta\ V_{dc}^{k+1}| \tag{4}$$

where,

$I_{\alpha-ref}^{k+1}, I_{\beta-ref}^{k+1}$	α-β axis reference current at k + 1 moment.
ΔV_{dc}	Voltage difference between upper and lower capacitance at k + 1 moment;
λ	Weighting factor of voltage balanced.

Based on above equations, the C-MPC method can be implemented in three-level inverter. Due to its simple algorithm and quickly dynamic response, it is widely used in power electronic field [25]. To the computation burden, this paper uses the PI control to replace the voltage balance control. So, the control scheme of C-MPC method in DSP is listed as follow.

However, C-MPC have some shortcoming, such as large output ripple [26], long computation time [11]. Compared with PWM modulation, C-MPC has worse steady state THD performance. Meanwhile, C-MPC has a big difference about output THD performance in different output current [26].

III. PROPOSED METHOD BASE ON VIRTUAL VECTOR WITH VARIABLE COEFFICIENT

To solve those problem of C-MPC, this paper proposed a MPC method based on virtual vector with variable coefficient (VC-VV-MPC method). It aims to improve the steady

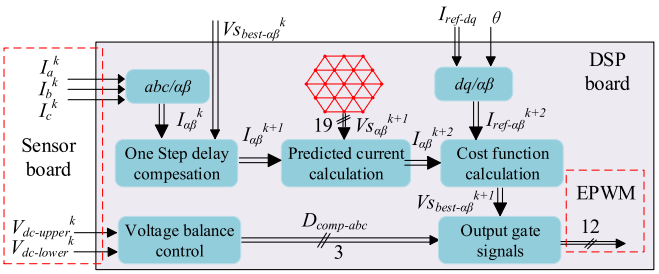

FIGURE 3. Control scheme of C-MPC method in DSP.

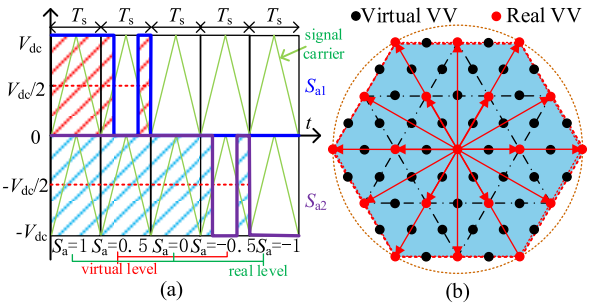

FIGURE 4. Diagram of virtual five-level space vector. (a) control pulse. (b) virtual five-level space vector.

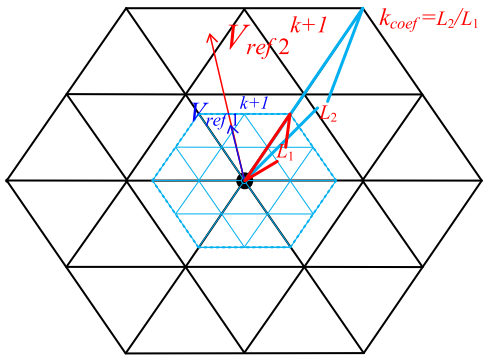

FIGURE 5. Vector distribution diagram at different reference current.

state performance and reduce the computation burden. To improve the steady state performance, this paper introduces five-level virtual vector into three-level converters through the principle of area equivalence. To further improve the closed-loop performance of the three-level NPC inverter, a variable coefficient is introduced so that the VV is distributed within the range of the three-level NPC inverter. After this, this paper uses the reference control voltage and VV pre-selection to reduce the computation time.

To expand the three-level space vector into a five-level space vector, the virtual level needs to be added, as shown in Fig. 4(a). When the virtual levels of $V_{dc}/2$ and $-V_{dc}/2$ are increased, the five-level space vector is shown in Fig. 4(b), and each red dot represents a real VV, and a black dot represents a virtual VV [24]. The control pulses of virtual and real levels are shown in Fig. 4(a), when Sa = 0.5, the Sa1 control signal is at a high level for half of the control period and the Sa2 is at a high level for the entire control period. For example, the initial VV is $V_s = \{1, 1, -1\}$ when a new VV $V_{new\_s} = \{0.5, 0.5, -0.5\}$ is needed, the transform coefficient is 0.5. This paper can use a coefficient to time the initial vector. Through the transformation step, all space vector of five-level can be calculated by three-level VVs. The expression is given by

$$\{S_{new\_a}, S_{new\_b}, S_{new\_c}\}^{5L} = \{d_a, d_b, d_c\} * \{S_a, S_b, S_c\}^{3L} \quad (5)$$

where,

$\{S_{new\_a}, S_{new\_b}, S_{new\_c}\}^{5L}$ Switching state of five-level voltage vector.
$\{d_a, d_b, d_c\}^{3L}$ Transform coefficient.
$\{S_a, S_b, S_c\}^{3L}$ Switching state of inverter.

The mathematical model of three-level NPC inverter output side in two-phase stationary reference frame is as follows

$$\begin{cases} Vs_\alpha = I_\alpha(R_o + R_L) + L\frac{dI_\alpha}{dt} \\ Vs_\beta = I_\beta(R_o + R_L) + L\frac{dI_\beta}{dt} \end{cases} \quad (6)$$

To apply the control algorithm to a discrete control system, it is necessary to discretize (6), where a first-order forward Euler discretization is used. The expression after the discretization is as follows

$$\begin{cases} V_{\text{ref}\_\alpha}^{k+1} = \frac{L}{T_s} I_{\alpha-ref}^{k+1} - \frac{L}{T_s} I_\alpha^{k+1}(1 - (R_o + R_L)T_s/L) \\ V_{\text{ref}\_\beta}^{k+1} = \frac{L}{T_s} I_{\beta-ref}^{k+1} - \frac{L}{T_s} I_\beta^{k+1}(1 - (R_o + R_L)T_s/L) \end{cases} \quad (7)$$

where

$I_{\alpha-ref}^{k+1}, I_{\beta-ref}^{k+1}$ α-β axis reference current at $k+1$ moment.
$V_{ref\_\alpha}^{k+1}, V_{ref\_\beta}^{k+1}$ α-β axis reference control VV at $k+1$ moment.

According to (7), when the system parameter is settled, with the changing the current reference, the selection of space vector changes. When the reference current $I_{\alpha\beta-ref}^{k+1}$ is very small, the reference control voltage $V_{\text{ref}}^{k+1}(V_{\text{ref}\_\alpha}^{k+1}, V_{\text{ref}\_\beta}^{k+1})$ is also small, so it is hard to find a suitable vector. Then the cost function will have a large deviation, make the converter have bad THD performance which is worse than 5%. This problem can be solved by sharing the same VV distribution between the high current reference and low current reference. As shown in the Fig. 6, to make different modulation index have the same THD performance, a variable coefficient is imported to make the two different modulations have the same VV distribution. When the current reference value is low, as shown by the blue line, while the red line indicates the higher current reference value. Where, $K_{\text{coef}} = L_2/L_1$, L_2 and L_1 are the maximum magnitudes of the two space vectors, respectively.

Based on the vector diagram of the maximum output range, when the output voltage is small, the reference control VV is calculated, and the coefficient of 125 vector V_{g125} is reduced to the new 125 vector $V_{g125}{}^{new}$ in equal proportion, so that it can meet the control situation of low modulation output, as shown in Fig. 5. The transformation is listed as

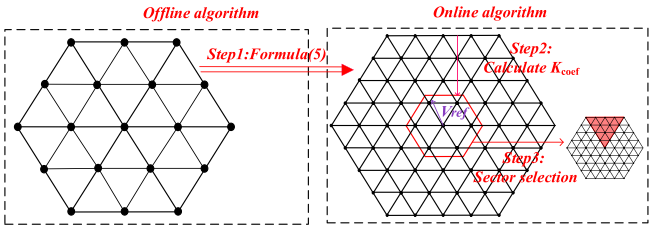

FIGURE 6. Schematic diagram of VV transformation.

follow, and the k_{coef} can be calculated by (9).

$$\left\{V_{g1}^{new}, \ldots, V_{g125}^{new}\right\} = \left\{V_{g1}, \ldots, V_{g125}\right\} K_{coef} \tag{8}$$

$$k_{coef} = |V_{ref-\alpha\beta}^{k+1}|/V_{dc} \tag{9}$$

where,

$\{V_{g1}, \ldots, V_{g125}\}$	Five-level VV;
$\{V_{g1}^{new}, \ldots, V_{g125}^{new}\}$	Variable coefficient five-level VV
$V_{ref-\alpha\beta}^{k+1}$	α-β axis converter voltage at k moment
K_{coef}	Coefficient
V_{dc}	DC bus voltage

This paper introduced the five-level space vector to three-level inverter, and the number of space vectors changes from 27 to 125. To reduce the computational burden, this paper deleted the redundant VV, and the reference control VV is calculated by (7). The sub-sector is determined by the angle of reference control VV. Therefore, the number of candidate VVs can be reduced to 15 at each control period.

The candidate vector selection process is shown in Fig. 6. The expansion of space vector is realized through (5). To improve the control performance, the scaling space vector $V_g{}^{new}$ is obtained through (8). The angle of the reference control VV is used to select the sub-sector and reduce the number of VVs to 15. The candidate VVs are obtained by multiplying the five-level space VV by K_{coef}, where the expression of K_{coef} is shown in (9).

After preselection of the candidate VVs, each candidate vector needs to be evaluated by the cost function. In C-MPC, the cost function is the tracking of the current reference value, as shown in (4). In this paper, the reference control VV is used to track, while eliminating the capacitor voltage balance term and the design of the weighting factors. The capacitor voltage balance is achieved by PI control. The expression of the cost function is given by

$$G = |V_{ref-\alpha\beta}^{k}{}^{+1} - V_g^{new}| \tag{10}$$

where, $V_g{}^{new}$ is the candidate VVs.

The control scheme of VC-VV-MPC is showed in Fig. 7. The control flow is summarized by the following steps.

Step 1) Measurement: sampling $i_a{}^k$, $i_b{}^k$, $i_c{}^k$, $V_{dc\_lower}{}^k$ and $V_{dc\_upper}{}^k$.

Step 2) Apply: the optimal VV $Vs_{best-\alpha\beta}{}^{k+1}$ at the pervious moment is applied to the three-level NPC inverter.

Step 3) Delay compensation: Predict $I_\alpha{}^{k+1}$ and $I_\beta{}^{k+1}$ to overcome the one-step delay caused by digital implementation.

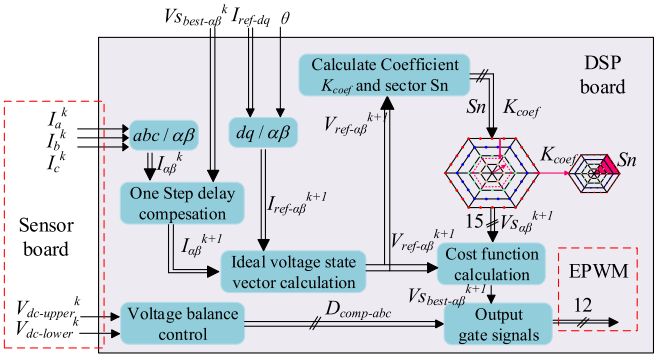

FIGURE 7. Control scheme of VC-VV-MPC method in DSP.

TABLE 1. Simulation parameter.

Parameter	Value
DC side voltage (V_{dc})	100 V
DC capacitor (C_{dc})	2000 μF
Filter inductance (L)	10 mH
Load resistor (R_O)	5 Ω
Line resistor (R_L)	3.6 Ω
Control period (T_s)	1 x 10^(-4) s
Output frequency (f_o)	50 Hz

Step 4) Reference control VV calculate: candidate reference control VV at $k + 1$ moment according to (7).

Step 5) Candidate VV pre-selection: The space vector is expanded by (5) and the scaled space vector is obtained by using (8) - (9). 15 VVs in the sub-sector were selected as candidate vectors according to the angle of the reference control VV.

Step 6) Cost function evaluation: The candidate VVs are brought into the cost function (10) for evaluation to obtain the optimal closed-loop action.

IV. SIMULATION ANALYSIS AND EXPERIMENTAL DATA ANALYSIS

Completed the introduction of the three methods, simulation and experiments were performed on the three methods to analyze their steady-state performance and dynamic response performance. After completing the simulation and experiment, an experimental platform of the three-level NPC inverter based on the TMS320F28379D controller was built to compare and analyze the dynamic response speed, steady-state output performance, computation and voltage balance of various methods. Finally, analyze the advantages and disadvantages of each of these methods.

A. SIMULATION AND DATA ANALYSIS

In this paper, C-MPC, AV-MPC, VC-VV-MPC method are simulated, analyzed and compared. This paper will compare with THD performance and the speed of response in simulation. This paper only will measure the computation in experiment due to the difficulty of measuring in simulation. The parameter of simulation is showed as Table 1.

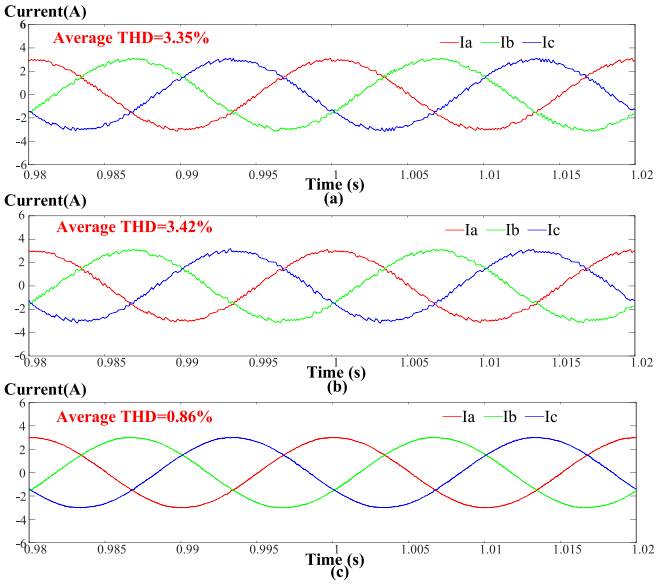

FIGURE 8. THD of 3A reference with three methods in simulation. (a) C-MPC method; (b) AV-MPC method; (c) VC-VV-MPC method.

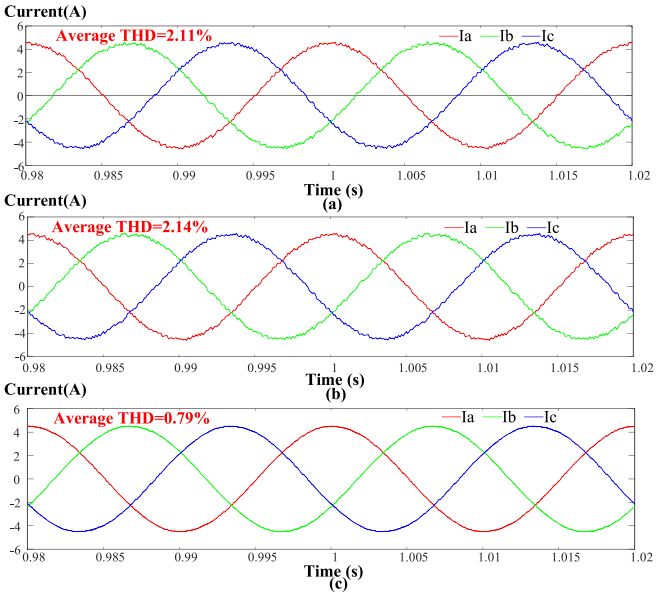

FIGURE 9. THD of 4.5A reference with three methods in simulation. (a) C-MPC method; (b) AV-MPC method; (c) VC-VV-MPC method.

The simulation results of different condition are showed as follow. As shown in Fig. 8 and Fig. 9, it is the THD analysis of three methods under different current output conditions. It can be seen from the Fig. 9 is that the VC-VV-MPC method have better THD performance compare with C-MPC and AV-MPC method under different load condition. Compared with the high current reference, the THD value of C-MPC and AV-MPC at the low current reference is larger and the performance is worse. However, the method of this paper can get the similar performance with high output current reference.

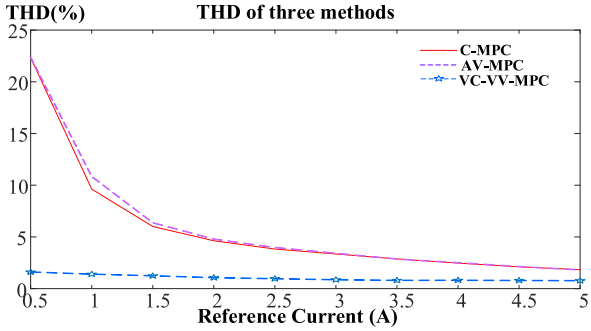

FIGURE 10. THD analysis with three methods in simulation.

TABLE 2. THD of multi-data with three control methods.

Ref. Current (A) / THD (%)	0.5	1	1.5	2	2.5	3	3.5	4	4.5	5
C-MPC	22.33	9.62	6.01	4.63	3.83	3.35	2.87	2.47	2.11	1.83
AV-MPC	22.35	10.84	6.37	4.79	3.98	3.42	2.86	2.51	2.14	1.8
VC-VV-MPC	1.61	1.4	1.24	1.06	0.96	0.86	0.8	0.81	0.79	0.77

To make THD analysis more convincing, this paper use multi current reference to do the data analysis. As shown in the Fig. 10, is the THD performance of multi data with three different methods. It can be seen from the Fig. 10 is that the C-MPC method and the AV-MPC method in Fig. 10 a have extremely poor output THD at low modulation degrees. The output performance of the high modulation degree section is better.

The THD of VC-VV-MPC in wide range of times of modulation degrees have the smallest value. Furthermore, a gentle trend within 2% is performed in VC-VV-MPC rather than obvious downward trend from 20% to 3% in C-MPC and AV-MPC. Therefore, the advantages of the variable coefficients proposed in this paper are verified in simulation.

All the detailed data are listed in the Table 2. The first row in Table 2 shows the magnitude of the reference current, and the second, third and fourth rows respectively correspond to the THD corresponding to different reference currents of three different methods.

As shown in Fig. 11, it is the dynamic response performance of three different methods. It can be seen from the Fig. 11 is that the three methods all have the similar dynamic response performance, but the VC-VV-MPC method is better.

Fig. 12 shows the capacitance balance waveforms of the three methods. The 0-0.2s stage is the start-up stage, the capacitance balance control is removed at 0.2-0.5s, and the capacitance voltage balance control is added at 0.5s −1s.

It can be seen that in the start-up stage, the three methods can balance the capacitor voltage. When the voltage balance control is lost, the voltages of C-MPC and AV-MPC have large deviation, the deviation of AV-MPC is larger, and the voltage fluctuation of VC-VV-MPC proposed in this paper is relatively small after losing voltage balance control. After

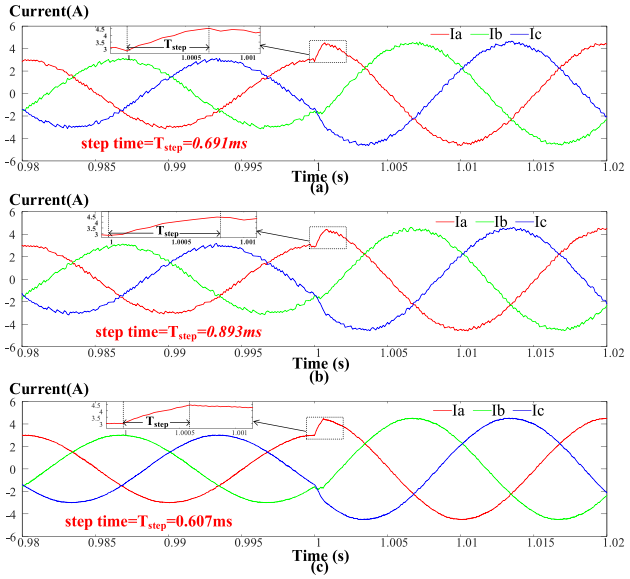

FIGURE 11. Dynamic response with three methods in simulation. (a) C-MPC method; (b) AV-MPC method; (c) VC-VV-MPC method.

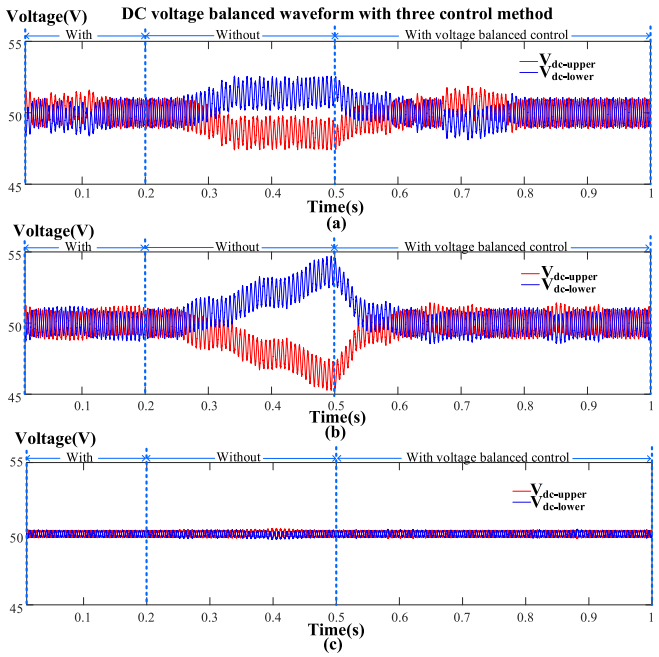

FIGURE 12. Voltage balanced waveform with three methods. (a) C-MPC method; (b) AV-MPC method; (c) VC-VV-MPC method.

adding capacitance balance control after 0.5s, the balance can be maintained again.

Regardless of the output THD performance or the dynamic response time, the performance of the control method based on VC-VV-MPC is better than the C-MPC method and AV-MPC method. In the case of capacitance voltage balance, VC-VV-MPC also has better performance. To prove the optimization of computation, it is necessary to measure the computation time of control algorithm. However, it is not convenient to collect the computation time in simulation.

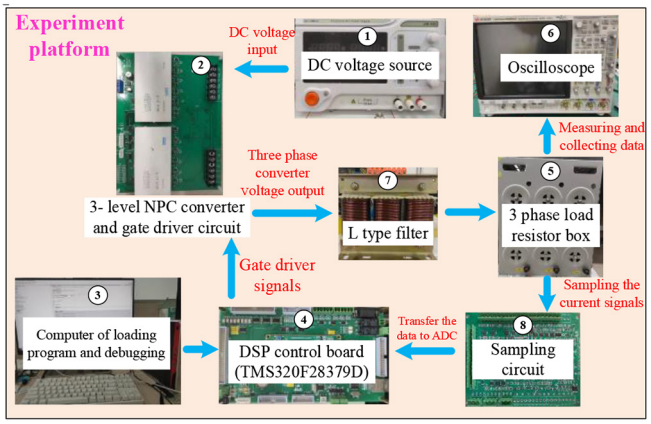

FIGURE 13. The structure of experiment platform.

TABLE 3. Experiment parameter settings.

Parameter	Value
DC voltage (V_{dc})	100 V
DC capacitor (C_{dc})	2000 μF
Filter inductance (L)	8.5 mH
Load resistor (R)	5 Ω
Line resistor (R_L)	3.6 Ω
Control period (T_s)	1 x 10^(-4) s
Output frequency (f_o)	50 Hz

Thus, this paper just showed the optimization result of computation in experiment.

B. EXPERIMENTAL DATA ANALYSIS

In order to prove the preliminary conclusion of simulation, this paper make a set of experiment platform of three-level NPC inverter based on TMS320F28379D control board. In this part, the C-MPC method, AV-MPC method and VC-VV-MPC method at different condition will compare by this experiment platform.

As showed in the Fig. 13, it is the experimental platform used in this paper, three-level NPC inverter experimental platform based on the TMS320F28379D control board. There are several parts: ① DC voltage source, ② three-level NPC inverter main circuit board plus drive circuit, ③ Computer, ④ TMS320F28379D control board, ⑤ load resistor box, ⑥ Oscilloscope, ⑦ L type filter, ⑧ Sampling board. The specific experimental parameters are shown in the Table 3.

In this paper, a passive oscilloscope probe is used to measure the real current waveform through the current sensor. The measurement ratio of the current sensor is 10 A - 5V. Two isolated probe is used to measure the upper and lower DC capacitor voltage. Finally, a passive oscilloscope probe is used to measure the output GPIO port waveform of the DSP to get calculation time. The parameters of the experimental platform are given in the Table 2. The test current condition is that the peak reference current is 3A and step to 4.5A after 2s.

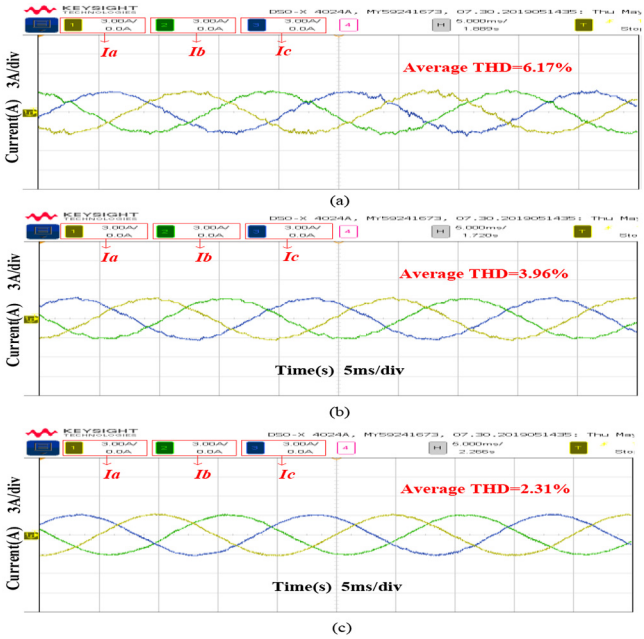

FIGURE 14. THD of 3A reference with three methods in experiment. (a) C-MPC method; (b) AV-MPC method; (c) VC-VV-MPC method.

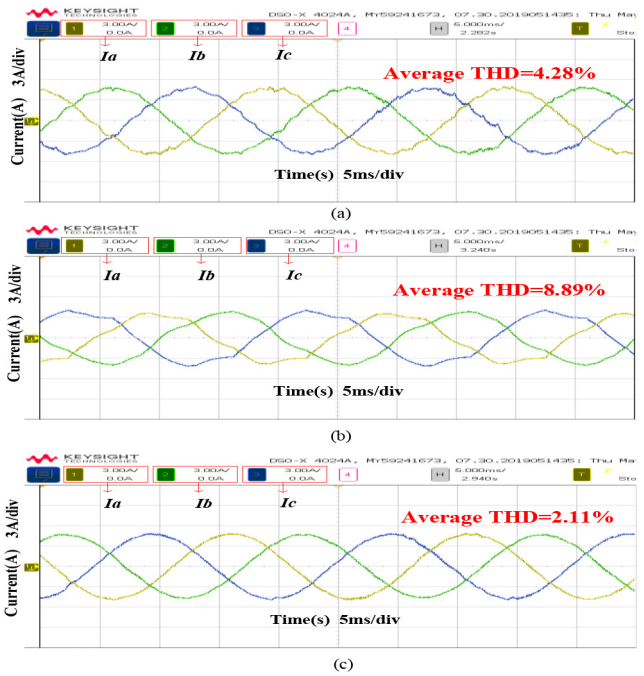

FIGURE 15. THD of 4.5A reference with three methods in experiment. (a) C-MPC method; (b) AV-MPC method; (c) VC-VV-MPC method.

As shown in Fig. 14 and Fig. 15, the steady-state three-phase currents at 3A and 4.5A output respectively, and their THD values are shown in the Fig. 14 and Fig. 15. It can be seen from the Fig. 14 is that, VC-VV-MPC and M-MPC method have better THD performance. The THD of low current reference is higher than the high current reference as the simulation. Meanwhile, different with the C-MPC

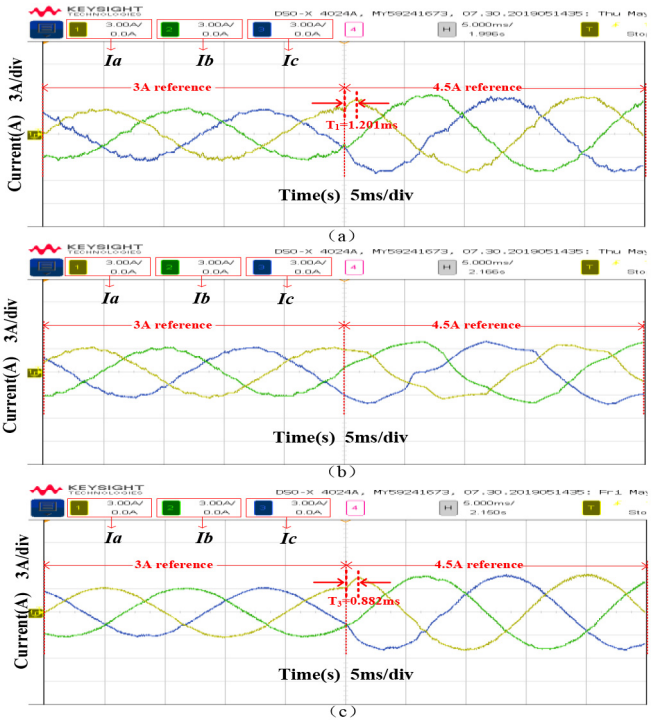

FIGURE 16. Dynamic response with three methods in experiment. (a) C-MPC method; (b) AV-MPC method; (c) VC-VV-MPC method.

and AV-MPC method, the VC-VV-MPC can keep the similar THD performance at different current reference. But the AV-MPC have some distortion due to it cannot output the current at high modulation range.

When the reference control current is increased from 3 A to 4 A, as shown in Fig. 16. Compare with other control strategy, the proposed method has faster dynamic response. In addition, the current THD of AV-MPC method increases significantly after the reference control current suddenly changes, because AV-MPC cannot achieve good control performance under high modulation

Fig. 17 shows the voltage balance waveform of three control algorithms. Compare with the C-MPC and AV-MPC methods, the proposed VC-VV-MPC method can effectively reduce the DC bus voltage fluctuation, which helps to reduce the current ripple.

Since the computation time is hard to count in the simulation, so this paper collected this data in the actual experiment platform. The calculation time can be collected by flipping the GPIO level at the control start point and the control end point. This GPIO output level is set to 1 when entering the control program, and it is set to 0 when exit the control program. As shown in Fig. 18, shows the computation of four different MPC method. It can be seen from the Fig. 18 is that, VC-VV-MPC have the smallest computation, next is the AV-MPC, the last one is C-MPC. The C-MPC cannot finished the control algorithm in one control period, so it let the control period longer. Other method all can finished the control algorithm in one control period.

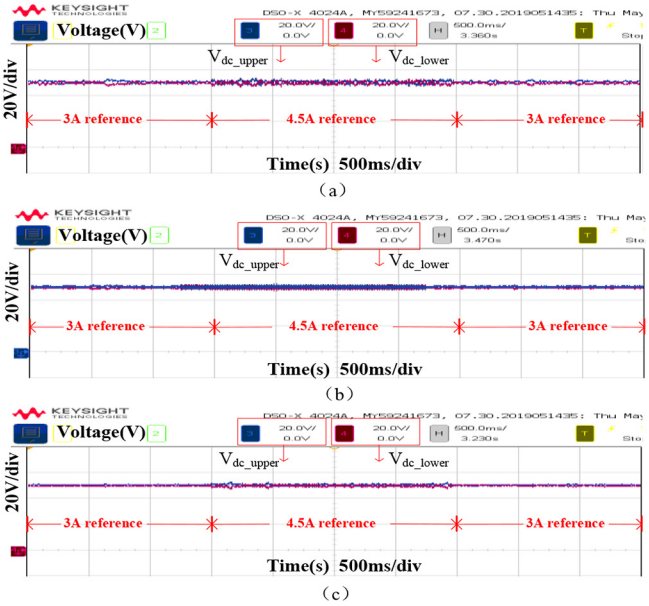

FIGURE 17. DC capacitor voltage waveform of three methods. (a) C-MPC method; (b) AV-MPC method; (c) VC-VV-MPC method.

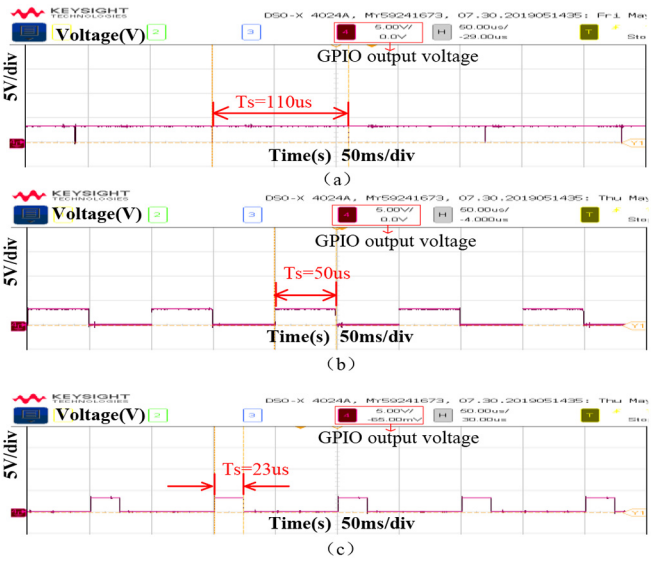

FIGURE 18. Comparison of calculation amount of three methods. (a)C-MPC method; (b)AV-MPC method; (c)VC-VV-MPC method.

TABLE 4. Comprehensive performance comparison of three methods.

Method	THD of 3A (%)	THD of 4.5A (%)	Step response (ms)	Voltage balance	Proportion of computa -tion (%)
C-MPC	6.17	4.28	1.201	yes	110%
AV-MPC	3.96	8.89	/	yes	50%
VC-VV-MPC	2.31	2.11	0.882	yes	23%

All the experimental data are shown in the Table 4. In theory, the AV-MPC should have the similar THD performance. However, in low modulation, the AV-MPC have better THD performance than the C-MPC, because the calculation amount of the C-MPC method in the actual situation has exceeded its control period, resulting in calculation overflow. And the VC-VV-MPC have best THD performance. In high modulation, due to the AV-MPC cannot output the correct current waveform, so the THD and step response is not useful. The VC-VV-MPC method still can keep best THD performance. Apart the AV-MPC method, all those methods can get a fast dynamic response performance, and all methods can keep voltage balanced. In the aspect of computation, VC-VV-MPC is the method of smallest computation.

V. CONCLUSION

The C-MPC control strategy applied to three-level NPC inverter has disadvantages such as high computational burden and large current ripple. To overcome these shortcomings, this paper proposes the VC-VV-MPC control strategy. The virtual five-level space vector is applied to the three-level NPC inverter, and the Coefficient is introduced to adjust the amplitude of the candidate vector, which can effectively improve the control performance in both low and high modulation range. The reference control voltage is used to select the appropriate candidate vectors, and the number of candidate vectors is reduced from 125 to 15, which greatly reduces the computational burden of the control algorithm. At the same time, the proposed DC bus voltage balance method can effectively reduce the bus voltage fluctuation. Simulation and experiments show that compared with C-MPC and AV-MPC control algorithms, the computational burden and control performance of the proposed algorithm are improved.

REFERENCES

[1] Q. X. Guan et al., "An extremely high efficient three-level active neutral-point-clamped converter comprising SiC and Si hybrid power stages," *IEEE Trans. Power Electron.*, vol. 33, no. 10, pp. 8341–8352, Oct. 2018.

[2] A. Deshpande, Y. Z. Chen, B. Narayanasamy, Z. Yuan, C. Chen, and F. Luo, "Design of a high-efficiency, high specific-power three-level T-type power electronics building block for aircraft electric-propulsion drives," *IEEE J. Emerg. Sel. Topics Power Electron.*, vol. 8, no. 1, pp. 407–416, Mar. 2020.

[3] S. Amamra, K. Meghriche, A. Cherifi, and B. Francois, "Multilevel inverter topology for renewable energy grid integration," *IEEE Trans. Ind. Electron.*, vol. 64, no. 11, pp. 8855–8866, Nov. 2017.

[4] H. D. Tafti, A. I. Maswood, G. Konstantinou, C. D. Townsend, P. Acuna, and J. Pou, "Flexible control of photovoltaic grid-connected cascaded H-bridge converters during unbalanced voltage sags," *IEEE Trans. Ind. Electron.*, vol. 65, no. 8, pp. 6229–6238, Aug. 2018.

[5] X. Wang et al., "Fault-tolerant control of common electrical faults in dual three-phase PMSM drives fed by T-type three-level inverters," *IEEE Trans. Ind. Appl.*, vol. 57, no. 1, pp. 481–491, Jan.-Feb. 2021.

[6] F. Donoso, A. Mora, R. Cárdenas, A. Angulo, D. Sáez, and M. Rivera, "Finite-set model-predictive control strategies for a 3L-NPC inverter operating with fixed switching frequency," *IEEE Trans. Ind. Electron.*, vol. 65, no. 5, pp. 3954–3965, May 2018.

[7] F. Sebaaly, H. Vahedi, H. Y. Kanaan, and K. Al-Haddad, "Novel current controller based on MPC with fixed switching frequency operation for a grid-tied inverter," *IEEE Trans. Ind. Electron.*, vol. 65, no. 8, pp. 6198–6205, Aug. 2018.

[8] A. Dekka, B. Wu, V. Yaramasu, and N. Zargari, "Model predictive control with common-mode voltage injection for modular multilevel converter," *IEEE Trans. Power Electron.*, vol. 32, no. 3, pp. 1767–1778, Mar. 2017.

[9] D. Xiao, K. S. Alam, and M. F. Rahman, "Predictive duty cycle control for four-leg inverters with LC output filter," *IEEE Trans. Ind. Electron.*, vol. 68, no. 5, pp. 4259–4268, May 2021.
[10] A. A. Ahmed, B. K. Koh, and Y. I. Lee, "A comparison of finite control set and continuous control set model predictive control schemes for speed control of induction motors," *IEEE Trans. Ind. Informat.*, vol. 14, no. 4, pp. 1334–1346, Apr. 2018.
[11] Y. Yang, H. Wen, M. Fan, M. Xie, and R. Chen, "Fast finite-switching-state model predictive control method without weighting factors for T-type three-level three-phase inverters," *IEEE Trans. Ind. Informat.*, vol. 15, no. 3, pp. 1298–1310, Mar. 2019.
[12] J.-H. Lee, J.-S. Lee, H.-C. Moon, and K.-B. Lee, "An improved finite-set model predictive control based on discrete space vector modulation methods for grid-connected three-level voltage source inverter," *IEEE J. Emerg. Sel. Topics Power Electron.*, vol. 6, no. 4, pp. 1744–1760, Dec. 2018.
[13] Y. Yang, H. Wen, M. Fan, M. Xie, R. Chen, and Y. Wang, "A constant switching frequency model predictive control without weighting factors for T-type single-phase three-level inverters," *IEEE Trans. Ind. Electron.*, vol. 66, no. 7, pp. 5153–5164, Jul. 2019.
[14] Z. Zhang, C. M. Hackl, and R. Kennel, "Computationally efficient DMPC for three-level NPC back-to-back converters in wind turbine systems with PMSG," *IEEE Trans. Power Electron.*, vol. 32, no. 10, pp. 8018–8034, Oct. 2017.
[15] M. Siami, D. A. Khaburi, M. Rivera, and J. Rodríguez, "A computationally efficient lookup table based FCS-MPC for PMSM drives fed by matrix converters," *IEEE Trans. Ind. Electron.*, vol. 64, no. 10, pp. 7645–7654, Oct. 2017.
[16] P. G. Ipoum-Ngome, D. L. Mon-Nzongo, R. C. C. Flesch, J. Song-Manguelle, M. Wang, and T. Jin, "Model predictive current control based on a generalized adjacent voltage vectors approach for multilevel inverters," *IET Power Electron.*, vol. 12, no. 13, pp. 3590–3599, Nov. 2019.
[17] D. Xiao, K. S. Alam, M. Norambuena, M. F. Rahman, and J. Rodriguez, "Modified modulated model predictive control strategy for a grid-connected converter," *IEEE Trans. Ind. Electron.*, vol. 68, no. 1, pp. 575–585, Jan. 2021.
[18] T. Liu, A. Chen, C. Qin, J. Chen, and X. Li, "Double vector model predictive control to reduce common-mode voltage without weighting factors for three-level inverters," *IEEE Trans. Ind. Electron.*, vol. 67, no. 10, pp. 8980–8990, Oct. 2020.
[19] Z. Ni, A. Abuelnaga, and M. Narimani, "A novel high-performance predictive control formulation for multilevel inverters," *IEEE Trans. Power Electron.*, vol. 35, no. 11, pp. 11533–11543, Nov. 2020.
[20] S. Xia, X. Wu, J. Zheng, X. Li, and K. Wang, "A virtual space vector PWM with active neutral point voltage control and common mode voltage suppression for three-level NPC converters," *IEEE Trans. Ind. Electron.*, vol. 68, no. 12, pp. 11761–11771, Dec. 2021.
[21] B. Hu, L. Kang, J. Liu, J. Zeng, S. Wang, and Z. Zhang, "Model predictive direct power control with fixed switching frequency and computational amount reduction," *IEEE J. Emerg. Sel. Topics Power Electron.*, vol. 7, no. 2, pp. 956–966, Jun. 2019.
[22] P. G. Ipoum-Ngome, D. L. Mon-Nzongo, R. C. C. Flesch, J. Song-Manguelle, M. Wang, and T. Jin, "Model-free predictive current control for multilevel voltage source inverters," *IEEE Trans. Ind. Electron.*, vol. 68, no. 10, pp. 9984–9997, Oct. 2021.
[23] C. R. Baier, R. O. Ramirez, E. I. Marciel, J. C. Hernández, P. E. Melín, and E. E. Espinosa, "FCS-MPC without steady-state error applied to a grid-connected cascaded H-bridge multilevel inverter," *IEEE Trans. Power Electron.*, vol. 36, no. 10, pp. 11785–11799, Oct. 2021.
[24] T. Jin, H. Song, D. L. Mon-Nzongo, P. G. Ipoum-Ngome, H. Liao, and M. Zhu, "Virtual three-level model predictive flux control with reduced computational burden and switching frequency for induction motors," *IEEE Trans. Power Electron.*, early access, Sep. 28, 2022, doi: 10.1109/TPEL.2022.3210388.
[25] C. F. Garcia, C. A. Silva, J. R. Rodriguez, P. Zanchetta, and S. A. Odhano, "Modulated model-predictive control with optimized overmodulation," *IEEE J. Emerg. Sel. Topics Power Electron.*, vol. 7, no. 1, pp. 404–413, Mar. 2019.
[26] N. Jin, M. Chen, L. Guo, Y. Li, and Y. Chen, "Double-vector model-free predictive control method for voltage source inverter with visualization analysis," *IEEE Trans. Ind. Electron.*, vol. 69, no. 10, pp. 10066–10078, Oct. 2022.

WEIQUAN GU received the B.S. degree in thermal energy engineering from Xi'an Jiaotong University, Xi'an, China, in 1996. He is now working with the Science and Technology Innovation Division, Fujian Fuqing Nuclear Power Company Ltd. His current research interests include thermal energy engineering, Intelligent electrical equipment, and energy router technology.

HUANGZHENG LIAO was born in Jiangxi province, China, in 1998. He received the B.S. degrees from East China Jiaotong University in 2019, and the M.S. degree from the Department of Electrical Engineering and Automation, Fuzhou University in 2022. His current research interests include the model predictive control, renewable power generation, and control of multilevel inverters.

JIAQI LIN was born in Fujian, China, in 1999. He received the B.S. degree in electrical engineering and automation from Huaqiao University, Xiamen, China, in 2021. He is currently pursuing the M.S. degree with the Department of Electrical Engineering and Automation, Fuzhou University, Fuzhou. His research interests include renewable power generation and topological structure of electronic and single-stage boost inverter.

ZEWEN LI was born in Fujian province, China, in 1996. He received the B.S. degrees from Fuzhou University in 2018, and the M.S. degree from the Department of Electrical Engineering and Automation, Fuzhou University in 2021. He is now working with State Grid Fujian Electric Power Research Institute. His current research interests include wireless power transfer, model predictive control, and distribution network.

TAO JIN (Senior Member, IEEE) received the B.S. and M.S. degrees in electrical engineering from Yanshan University, Qinhuangdao, China, in 1998 and 2001, respectively, and the Ph.D. degree in electrical engineering from Shanghai Jiaotong University, Shanghai, China, in 2005. From 2005 to 2007, he worked as a Postdoctoral Fellow with Shanghai Jiaotong University. From 2008 to 2009, he was a Research Scientist position with Virginia Tech, Blacksburg, VA, USA. In 2010, he joined Imperial College London, London, U.K., as a European Union Marie Curie Research Fellow, where he focused on electrical technologies related to smart grid. He is currently a Professor with the College of Electrical Engineering and Automation, Fuzhou University, Fuzhou, China. He has authored about 160 articles. He is a member of the IEEE Power and Energy Society and the IEEE Industrial Electronics Society, and a Special Committee Member of the Chinese Society of Electrical Engineering and the China Electrotechnical Society. He currently serves as an Associate Editor for *Modern Power Systems and Clean Energy*, *Protection and Control of Modern Power Systems*, *China Measurement and Testing Technology*, and other journals.